THE JOURNAL OF BIOLOGICAL CHEMISTRY VOL. 291, NO. 20, pp. 10490–10500, May 13, 2016

Ectodomain Shedding of Lymphatic Vessel Endothelial Hyaluronan Receptor 1 (LYVE-1) Is Induced by Vascular Endothelial Growth Factor A (VEGF-A)*

Received for publication, August 3, 2015, and in revised form, March 7, 2016 Published, JBC Papers in Press, March 10, 2016, DOI 10.1074/jbc.M115.683201

Hisayo Nishida-Fukuda[‡§], Ryoichi Araki[‡], Masachika Shudou[¶], Hidenori Okazaki[‡], Yasuko Tomono[‖], Hironao Nakayama[§‡‡], Shinji Fukuda[§‡‡], Tomohisa Sakaue[§‡‡], Yuji Shirakata[‡], Koji Sayama[‡], Koji Hashimoto[‡], Michael Detmar[§§], Shigeki Higashiyama[§**‡‡], and Satoshi Hirakawa[‡**¶¶1]**

*From the Departments of [‡]Dermatology, [§]Biochemistry and Molecular Genetics, and [¶]Bioscience, Advanced Research Support Center (ADRES), Ehime University Graduate School of Medicine, Toon 791-0295, Japan, [‖]Division of Molecular and Cell Biology, Shigei Medical Research Institute, Okayama 701-0202, Japan, **Strategic Young Researcher Overseas Visiting Program for Accelerating Brain Circulation, Japan Society for the Promotion of Science (JSPS), 5-3-1 Kojimachi, Chiyoda-ku, Tokyo 102-0083, Japan, [‡‡]Division of Cell Growth and Tumor Regulation, Proteo-Science Center (PROS), Ehime University, Toon 791-0295, Japan, [§§]Institute of Pharmaceutical Sciences, Swiss Federal Institute of Technology, ETH Zurich, Zurich CH-8093, Switzerland, and [¶¶]Department of Dermatology, Hamamatsu University School of Medicine, Hamamatsu 431-3192, Japan*

Lymphatic vessel endothelial hyaluronan receptor 1 (LYVE-1), a type I transmembrane glycoprotein, is known as one of the most specific lymphatic vessel markers in the skin. In this study, we found that the ectodomain of LYVE-1 undergoes proteolytic cleavage, and this process produces soluble LYVE-1. We further identified the cleavage site for ectodomain shedding and generated an uncleavable mutant of LYVE-1. In lymphatic endothelial cells, ectodomain shedding of LYVE-1 was induced by vascular endothelial growth factor (VEGF)-A, an important factor for angiogenesis and lymphangiogenesis under pathological conditions. VEGF-A-induced LYVE-1 ectodomain shedding was mediated via the extracellular signal-regulated kinase (ERK) and a disintegrin and metalloproteinase (ADAM) 17. Wild-type LYVE-1, but not uncleavable LYVE-1, promoted migration of lymphatic endothelial cells in response to VEGF-A. Immunostaining analyses in human psoriasis skin lesions and VEGF-A transgenic mouse skin suggested that the ectodomain shedding of LYVE-1 occurred in lymphatic vessels undergoing chronic inflammation. These results indicate that the ectodomain shedding of LYVE-1 might be involved in promoting pathological lymphangiogenesis.

Lymphatic vessels play crucial roles in maintaining tissue fluid homeostasis, immune surveillance, and fat absorption. Physiological lymphangiogenesis is regulated by several genes including Prox1 and vascular endothelial growth factor (VEGF)-C that induce the sprouting of lymphatic endothelial cells from embryonic veins during mammalian development (1, 2). Lymphatic endothelial cells express VEGF receptors (VEGFRs)[2] that represent a family of receptor tyrosine kinases. Among them, VEGFR-3 plays an essential role in promoting physiological lymphangiogenesis because VEGFR-3 shows a high affinity toward VEGF-C. In fact, several missense mutations are known among tyrosine kinase domains in *Flt4*/*VEGFR-3* that lead to the formation of Milroy disease, a congenital lymphedema due to an insufficient development of cutaneous lymphatic vessels. Thus, the VEGF-C/VEGFR-3 pathway plays a crucial role in promoting physiological and pathological lymphangiogenesis.

VEGF-A, a specific ligand for VEGFR-1 and VEGFR-2, induces cutaneous angiogenesis in physiological and pathological conditions such as psoriasis (3). Targeted overexpression of mouse VEGF-A164 in the epidermis of transgenic mice leads to the formation of erythematous plaques resembling psoriasis (4), indicating that VEGF-A plays an important role in the pathogenesis of psoriasis. Our previous studies indicated that targeted overexpression of VEGF-A in mouse skin promotes the prominent enlargement of lymphatic vessels during acute inflammation by ultraviolet-B irradiation (5) and induces tumor-associated lymphangiogenesis as well as angiogenesis during multistep chemically induced skin carcinogenesis (6). Importantly, tumor lymphangiogenesis actively promotes enhanced metastasis to draining lymph nodes and beyond in VEGF-A transgenic mice as compared with wild-type littermates. Ectopic expression of human VEGF-A165 in mouse skin resulted in the formation of giant lymphatic vessels via the activation of VEGFR-2 (7). Recently, homozygous overexpression

* This work was supported by Grants-in-aid for Scientific Research B23390283 and 26293257 from the Ministry of Education, Culture, Sports, Science, and Technology of Japan (to S. Hirakawa), Grant-in-aid for Scientific Research H223G008B1 from the Ministry of Health, Labor, and Welfare of Japan (to S. Hirakawa), Grant-in-aid for Scientific Research on Priority Areas MEXT18013037 and MEXT20013032 (to S. Hirakawa), and Japan Agency for Medical Research and Development Practical Research Project for Rare/Intractable Diseases Grant 15ek0109057h0002 (to S. Hirakawa). The authors declare that they have no conflicts of interest with the contents of this article.

[1] To whom correspondence should be addressed: Dept. of Dermatology, Hamamatsu University School of Medicine, Handayama 1-20-1, Higashi-ku, Hamamatsu 431-3192, Japan. Tel.: 81-53-435-2065; Fax: 81-53-435-2368; E-mail: hirakawa@hama-med.ac.jp.

[2] The abbreviations used are: VEGFR, VEGF receptor; LYVE-1, lymphatic vessel endothelial hyaluronan receptor 1; ADAM, a disintegrin and metalloproteinase; TPA, phorbol ester 12-*o*-tetradecanoylphorbol-13-acetate; AP, alkaline phosphatase; LEC, lymphatic endothelial cell; PV, plasmalemmal vesicle-associated protein; NHS, *N*-hydroxysuccinimide; HUVEC, human umbilical vein endothelial cell; CTF, C-terminal fragment; TACE, TNF-α-converting enzyme.

of VEGF-A in mouse skin further demonstrated that the prominent enlargement of cutaneous lymphatic vessels is induced by spontaneous chronic inflammation in the transgenic mice (8). Of particular interest, the fluid transport of cutaneous lymphatic vessels was markedly impaired in the VEGF-A transgenic mice, indicating that the epidermal overexpression of VEGF-A alters the physiological function of cutaneous lymphatic vessels and promotes pathological lymphangiogenesis. However, it remains unclear whether lymphatic vessels are functionally altered at the cellular level in VEGF-A transgenic mice.

The lymphatic vessel endothelial hyaluronan receptor 1 (LYVE-1), a type I transmembrane glycoprotein, is one of the most reliable markers for cutaneous lymphatic vessels. LYVE-1 has a hyaluronan-binding motif in the N-terminal sequence, whereas the cytoplasmic domain of LYVE-1 corresponds to the C-terminal polypeptide sequence (9). The deduced amino acid sequence of LYVE-1 predicted a 322-residue polypeptide that is similar to CD44, the leukocyte hyaluronan receptor, by 41% (9). LYVE-1 is known to localize in the initial lymphatic vessels in the skin and is specifically expressed by the lymphatic endothelial cells (LECs) (10, 11). Although previous studies in LYVE-1 knock-out mice found no specific phenotype with regard to lymphangiogenesis (12, 13), it remains unclear whether post-translational modifications of LYVE-1 might play functional roles in pathological conditions such as psoriasis.

Ectodomain shedding, the proteolytic cleavage of a transmembrane protein, is triggered by multiple stimulations such as extracellular calcium influx and activation of protein kinase C and other signaling pathways (14, 15). Ectodomain shedding is mediated through the activation of metalloproteases in several cell lineages including endothelial cells (15, 16). Importantly, CD44 is proteolytically cleaved at the extracellular domain through membrane-associated metalloproteases (17). However, it remains unclear whether LYVE-1 undergoes ectodomain shedding in response to lymphangiogenesis factors such as VEGF ligands.

In this study, we provide evidence, for the first time, that LYVE-1 is proteolytically cleaved from LECs in response to VEGF-A. Analysis of human psoriasis tissues and VEGF-A transgenic mouse skin revealed a possibility that LYVE-1 shedding arises in lymphatic vessels undergoing chronic inflammation. These results suggest that LYVE-1 might contribute to promoting pathological lymphangiogenesis in the skin.

Experimental Procedures

Reagents—Recombinant human VEGF-A165, VEGF-C, and VEGF-D were purchased from R&D Systems. U0126 was purchased from Cell Signaling Technology. KB-R7785 was a gift from Carna Biosciences Inc. Phorbol ester 12-*o*-tetradecanoylphorbol-13-acetate (TPA) was purchased from Wako. Rabbit polyclonal anti-LYVE-1 antibody (ab10278) and rabbit polyclonal anti-LYVE-1 (biotin) antibody (ab37288) were purchased from Abcam. Mouse monoclonal anti-β-actin antibody (A5441) was purchased from Sigma. Rabbit polyclonal anti-LYVE-1 antibody (PA1-16636) was purchased from Affinity BioReagents. Rabbit polyclonal anti-TACE/a disintegrin and metalloproteases (ADAM) 17 antibody (PC491) was purchased from Chemicom International. Mouse monoclonal anti-claudin-5 antibody (35-2500) and mouse monoclonal anti-V5 antibody (R960-25) were purchased from Invitrogen. Rabbit monoclonal anti-ERK1/2 antibody (4695), anti-phospho-ERK1/2 Thr^{202}/Tyr^{204} antibody (4370), anti-VEGFR-2 antibody (2479), and anti-phospho-VEGFR-2 Tyr^{1175} antibody (2478) were purchased from Cell Signaling Technology.

Animals—Homozygous K14/VEGF-A transgenic mice express the coding sequence of mouse VEGF-A164 under control of the keratin-14 promoter on the FVB/N genetic background (4). Transgenic and wild-type female mice used in this study were 20 weeks post-birth. All animal studies were approved by the Ehime University Graduate School of Medicine Subcommittee on Research Animal Care.

Immunofluorescence Analyses—For immunofluorescence analyses, ears were removed after mice were euthanized. For section staining, skin samples were embedded in optimal cutting temperature (OCT) compound (Sakura Finetek) and snap frozen. Cryostat sections were immunostained as described previously with antibodies against mouse plasmalemmal vesicle-associated protein (PV)-1 or LYVE-1 (6, 18). For whole-mount staining, ears were surgically opened into two flaps and fixed for 30 min in 4% paraformaldehyde. After permeabilization with 0.5% Triton X-100, tissues were stained using antibodies against mouse claudin-5 or LYVE-1. The respective secondary antibodies were labeled with Alexa Fluor 488 or 594 (Molecular Probes). Nuclei were counterstained with 4′,6′-diamidino-2-phenylindole (DAPI) (Molecular Probes). Digital images of sections and tissues were captured using a confocal laser scanning microscope (A1, Nikon).

Scanning Electron Microscopy and Transmission Electron Microscopy—The animals were anesthetized by intraperitoneal injection of pentobarbital sodium and perfused through the left ventricle with physiological saline and then with a fixative containing 2.5% glutaraldehyde in 0.1 M cacodylate buffer (pH 7.4). The earlobe was then removed, cut into short loops, and immersed in the same fixative for 1 day at 4 °C. To remove the connective tissue elements of the earlobe, the specimens were placed in 30% KOH for 5–10 min at 60 °C and washed in 0.1 M cacodylate buffer (pH 7.4). Then the tissues were put in an aqueous solution of tannic acid for 3–4 h, rinsed in distilled water several times, and stained with 2% OsO_4 solution for 3 h at 4 °C. Next, they were dehydrated through a graded series of ethanol, transferred to *t*-butyl alcohol, and subjected to *t*-butyl alcohol freeze-drying. The dried tissues were dissected with a needle and forceps under a binocular dissected microscope and mounted on aluminum stubs. These samples were then coated with osmium (HPC-30W Plasma Coater, Vacuum Device Inc.) and studied by scanning electron microscopy (Hitachi S-4800) at an accelerating voltage of 2 kV. For transmission electron microscopy, specimens fixed in the same fixative as above were postfixed for 2 h with 1% OsO_4 solution in 0.1 M cacodylate buffer (pH 7.4), dehydrated through a graded series of ethanol, and embedded in Epon 812. Ultrathin sections were stained with uranyl acetate and lead citrate and studied using a transmission electron microscope (JEM-1230, JEOL) at an accelerating voltage of 80 kV.

TABLE 1
Sequences of primer sets for PCR
FK/AA, F226A/K227A; NE/AA, N228A/E229A.

No.	Plasmid name	Forward primer sequences (5′–3′)	Reverse primer sequences (5′–3′)
1	AP-hLYVE1	AATCTCGAGGCAGAAGAGCTTTCCATCCA	ATTCTAGACTAAACTTCAGCTTCCAGGCATCG
2	hLYVE1 FLAG1	GATGATGACAAGGGCTTTATGGAAACTAGCACCAT	GTCCTTGTAGTCTCTCCGTGGAATAGAAGTGG
3	hLYVE1 FLAG2	GATGATGACAAGGGCGGGTTTGGAGGTGTCCCCAC	GTCCTTGTAGTCATTTTCAACAAATGGTTCAG
4	LYVE1 Δ226–229	GCTGCTGGGTTTGGAGGTGT	TGCTGCTTTATTTTCAACAAATGGTTCAG
5	LYVE1 F226A	AAGAATGAAGCTGCTGGGTTTG	GGCTGCTGCTTTATTTTCAACAAAT
6	LYVE1 K667A a	GAATTCGTCGACAGATCTGCCACCATGGCCAAGTGC	GACCAGCTGCAGCACCAAAGAAGAGGAGAG
7	LYVE1 K667A b	AAAGCAGCATTCGCGAATGAAGCTGCTGGG	TCTAGATTACGTAGAATCGAGACCGAGGAG
8	LYVE1 N228A	GAAGCTGCTGGGTTTGGAGG	AGCCTTGAATGCTGCTTTATTTTC
9	LYVE1 E229A	GCAGCTGCTGGGTTTGGAG	ATTCTTGAATGCTGCTTTATTTTC
10	LYVE1 FK/AA	GCGAATGAAGCTGCTGGGTTTG	GGCTGCTGCTTTATTTTCAACAAAT
11	LYVE1 NE/AA	GCAGCTGCTGGGTTTGGAG	AGCCTTGAATGCTGCTTTATTTTC
12	ADAM8	ACCCGGCAGGCACCAAA	CCAAGGCGGGGAGAAGGAAT
13	ADAM9	TCTCTGGCAATGAATACAAG	ACAGACAATAAGGGGAACA
14	ADAM10	TCATGGTGAAACGCATAAGAA	ACAGTCTGAATCATCCCGACA
15	ADAM12	CGTGTTGGTAGGCGTGGAA	TGACATGAGTGCCCATCGTG
16	ADAM15	CCAGCCCCAGCCAAGACCT	GTGCCCAGCCCTCCTCACAG
17	ADAM17/TACE	GGCAAAAAGTTACCCAAATG	CAATGAAATCCCAAAATCGT

Cell Culture—The fibrosarcoma cell line HT1080 was cultured in DMEM supplemented with 10% fetal bovine serum (FBS). Neonatal human dermal lymphatic microvascular endothelial cells (HMVEC-dLys Neo) were purchased from Lonza and grown in an EGM-2-MV bullet kit (Lonza). The endothelial cells were used at passages 4–6.

Plasmid Construction—The human LYVE-1 cDNA was obtained from Life Technologies. The fragments of alkaline phosphatase (AP)-tagged LYVE-1 and LYVE-1 mutants were constructed by PCR using the Expand High Fidelity PCR system (Roche Applied Science) or KOD Plus DNA polymerase (Toyobo), and cloned into the pME18S vector or pcDNA3.1+ vector. Primer sequences are given in Table 1.

Cell Surface Biotinylation—Cells were washed twice with ice-cold PBS and incubated on ice with 0.1 mg/ml sulfo-NHS-biotin (Pierce) in 0.1 M HEPES, 0.15 M NaCl (pH 8.0) for 15 min. To quench the biotinylation reaction, the cells were washed with ice-cold growth medium. The cells were washed twice with ice-cold PBS and then lysed with radioimmune precipitation assay buffer (50 mM Tris HCl (pH 7.5), 150 mM NaCl, 1% Nonidet P-40, 0.1% SDS, 0.5% sodium deoxycholate) supplemented with Complete protease inhibitor mixtures (Sigma). The cell lysates were subjected to immunoprecipitation using anti-V5 antibody (Invitrogen). After SDS-PAGE and Western blotting, cell surface LYVE-1 was detected by horseradish peroxidase (HRP)-conjugated streptavidin (Vector Laboratories).

AP-tagged LYVE-1 Shedding Assay—HT1080 cells transfected with AP-tagged LYVE-1 or AP-tagged LYVE-1 mutants were stimulated by TPA for 30 min. LECs transduced with adenovirus encoding AP-tagged LYVE-1 and AP-tagged LYVE-1 uncleavable mutant were incubated with the starvation medium (endothelial cell basal medium with 0.5% FBS) for 6 h. The cells were treated with or without VEGF-A165 (50 ng/ml) for 6 h. KB-R7785 or U0126 was added 30 min prior to VEGF-A165 stimulation. The conditioned media were collected and heated for 15 min at 65 °C to inactivate endogenous AP. An equal volume of a 2× AP buffer (2 M diethanolamine (pH 9.8), 1 mM $MgCl_2$, 20 mM L-homoarginine, 24 mM *p*-nitrophenyl phosphate) was added. AP activity was determined by measuring the absorbance at 405 nm with an ARVO multilabel counter (PerkinElmer Life Sciences). Three independent experiments were performed for each assay. Statistical analyses were performed using the unpaired Student's *t* test.

Adenovirus Construction and Transduction—Adenovirus vectors encoding LYVE-1, AP-LYVE-1, and AP-LYVE-1 uncleavable mutant were prepared using an adenovirus expression kit (Takara Bio Inc.). LECs were transduced with purified, concentrated, and titer-checked viruses at a multiplicity of infection of 100. The construction and transduction of adenovirus vectors were approved by the institutional review board of Ehime University Graduate School of Medicine.

RNA Interference—siGENOME SMARTpool small interfering RNA (siRNA) against ADAM17 (Dharmacon) was introduced into LECs using Lipofectamine RNAiMAX (Invitrogen). siGENOME Non-targeting siRNA was used as a negative control. For rescue experiments, HUVECs were transfected with AP-LYVE-1, ADAM17-FLAG, or empty vector using X-tremeGENE HP DNA transfection reagent (Roche Applied Science). Then ADAM17 siRNA (SASI_Hs01_00027258, Sigma) or control siRNA (Mission_SIC_001s/Mission_SIC_001as) was introduced using Lipofectamine RNAiMAX. Cells were grown for 48 h after transfection and then subjected to the AP-tagged LYVE-1 shedding assay. Knockdown efficiency was validated by a TaqMan gene expression assay (Applied Biosystems) and Western blotting analysis. Three independent experiments were performed for each assay.

Cell Migration Assay—LECs, after transduction of the wild-type or uncleavable form of LYVE-1, were seeded in serum-free endothelial cell basic medium-2 containing 0.2% delipidated BSA into the upper chambers of FluoroBlok inserts (Falcon). The underside of the filters was precoated with 1 mg/ml hyaluronan (Wako). LECs were preincubated for 30 min in the presence or absence of KB-R7785 and further incubated for 3 h at 37 °C in the presence or absence of VEGF-A165 (50 ng/ml) in the bottom well. Cells on the underside of the inserts were stained with 4′,6-diamidino-2-phenylindole (DAPI) (Sigma), and the number of migrated cells was counted in three random 10× fields per well. Three independent experiments were performed for each assay. Statistical analyses were performed using the unpaired Student's *t* test.

Tissue Collection—All human tissue samples were obtained with informed consent in accordance with the approval by the

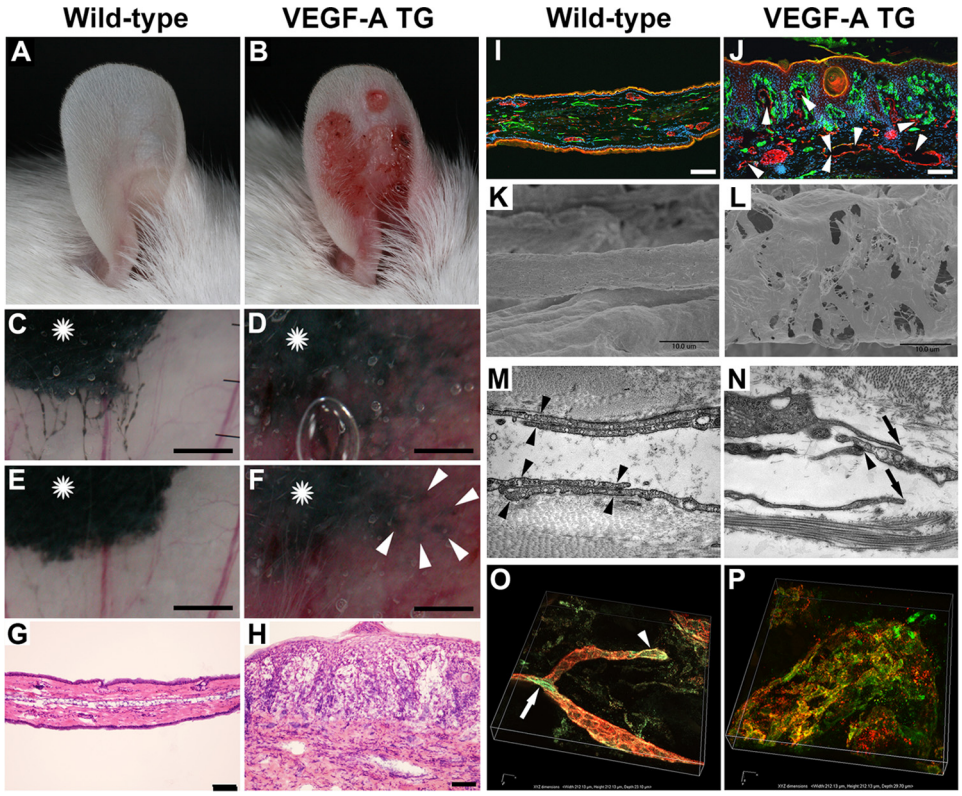

FIGURE 1. **Targeted overexpression of VEGF-A in mouse skin is associated with extracellular localization of LYVE-1.** *A* and *B*, wild-type littermates show normal ear skin (*A*), whereas targeted overexpression of VEGF-A leads to erythematous plaques resembling psoriasis (*B*). *C–F*, colloidal carbon injection (*asterisk*) into the ears revealed that VEGF-A overexpression impaired fluid transport by cutaneous lymphatic vessels (*F*, *arrowheads*). Respective images indicate 5 (*C* and *D*) or 30 min (*E* and *F*) after injection. *Scale bar*, 1 mm. *G–J*, H&E and double immunofluorescence staining for blood (PV-1; *green*) and lymphatic vessels (LYVE-1; *red*) shows prominent expansion of lymphatic vessels without continuous vessel wall in VEGF-A transgenic mice (*J*, *arrowheads*). Nuclei were stained by DAPI (*blue*). *Scale bar*, 100 μm. *K–N*, electron microscopic analyses showed that VEGF-A overexpression leads to fenestration of initial lymphatics that sometimes lack overlap of lymphatic endothelial cells (*N*, *arrows*). *Scale bar*, 100 μm. *O* and *P*, three-dimensional confocal microscopic images of LYVE-1 (*red*) and claudin-5 (*green*) show prominent extracellular localization of LYVE-1 in VEGF-A transgenic mice. *TG*, transgenic.

research ethics committee at Ehime University Graduate School of Medicine.

Preparation of Monoclonal Antibody—Monoclonal antibody was generated according to a previous report (19). Briefly, WKY/Ncrj rats (Charles River, Japan) were immunized with emulsion containing a keyhole limpet hemocyanin-conjugated LYVE-1 C-terminal fragment (CTF) synthetic peptide (Lys^{260}–Val^{322}) and Freund's complete adjuvant. Rat lymph node cells were fused with mouse myeloma Sp2/0 cells. The hybridomas were screened using ELISA, and clone CTF1-2 was selected. The monoclonal antibody was suitable for ELISA and immunofluorescence but not for Western blotting analysis.

ELISA—An ELISA plate (Nunc) was coated with LYVE-1 CTF or CD44 CTF peptide. After blocking with 1% bovine serum albumin, the plate was incubated with the conditioned media of hybridomas. After washing with PBS, the plate was incubated with HRP-conjugated anti-rat antibody. *O*-Phenylenediamine (Wako) was used with HRP substrate.

Results

Targeted Overexpression of VEGF-A in Mouse Skin Showed the Extracellular Localization of LYVE-1—Pathological production of VEGF-A promotes cutaneous angiogenesis in several skin diseases such as psoriasis (3) and in experimental animal models (4). In wild-type mice, ear skin remains normal (Fig. 1*A*), whereas targeted overexpression of VEGF-A in mouse skin promotes the development of erythematous plaques resembling psoriasis (Fig. 1*B*). To elucidate the characteristics of lymphatic vessels in VEGF-A transgenic mice, colloidal carbon was injected into the ear skin. Dermoscopy images at 5 min after the injection showed that cutaneous lymphatic vessels transported colloidal carbon away from the injection site in wild-type littermates (Fig. 1*C*), whereas this transport was completed after 30 min when no draining lymphatic vessels were seen (Fig. 1*E*). In contrast, in VEGF-A transgenic mice, the cutaneous lymphatic vessels that transported colloidal carbon were markedly enlarged at 5 min after the injection (Fig. 1*D*). Importantly, VEGF-A overexpression impaired fluid transport by cutaneous lymphatic vessels because dilated pigmented lymphatic vessels were still visible after 30 min (Fig. 1*F*, *arrowheads*). Hematoxylin-eosin staining revealed normal ear skin in wild-type mice (Fig. 1*G*), whereas VEGF-A overexpression resulted in epidermal hyperplasia (Fig. 1*H*). We next investigated the effect of chronic VEGF-A overexpression on lymphatic and blood vessels by immunofluorescence staining using antibodies against LYVE-1 for red and PV-1, a blood vessel-specific marker, for green. We found that vascularization was increased in VEGF-A transgenic mice as compared with wild-type littermates (Fig. 1, *I* and *J*), indicating that the targeted

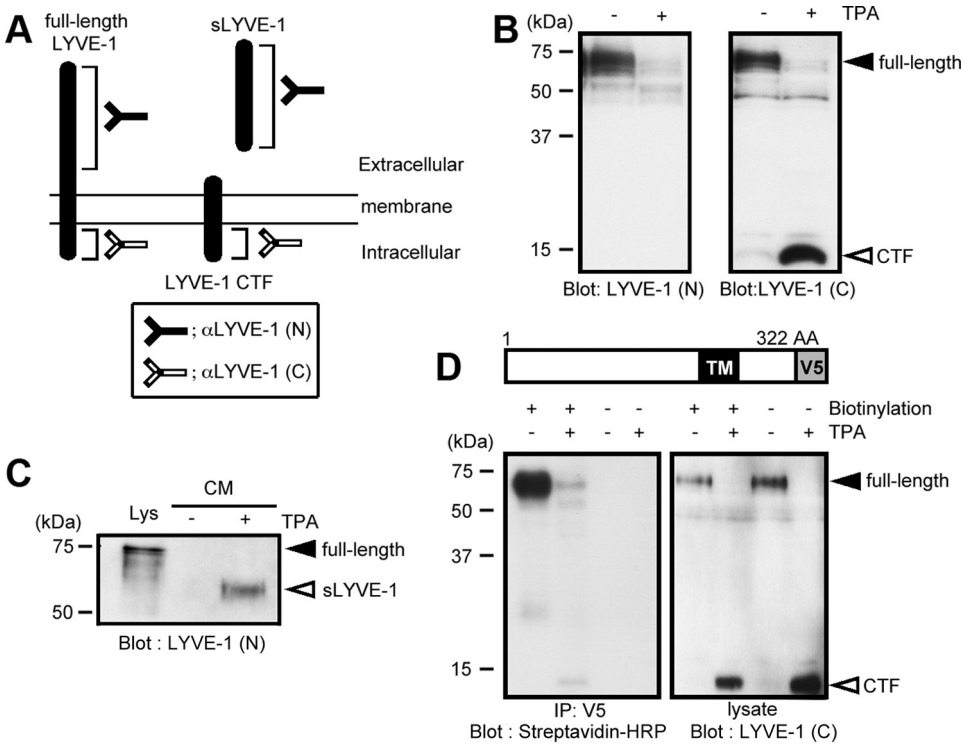

FIGURE 2. **LYVE-1 ectodomain shedding.** *A*, schematic representation of LYVE-1 cleavage product detection by two antibodies. Anti-LYVE-1 (C) antibody can recognize not only full-length LYVE-1 but also LYVE-1 CTF generated by LYVE-1 ectodomain shedding. Anti-LYVE-1 (N) antibody can recognize full-length and soluble LYVE-1 (*sLYVE-1*). *B*, Western blotting analysis of cell lysates derived from LYVE-1-transfected HT1080 cells. After TPA treatment (100 nM) for 30 min, the cell lysates were detected by anti-LYVE-1 (C) or anti-LYVE-1 (N) antibody. Five micrograms of total cellular protein was loaded in each gel lane. *C*, detection of sLYVE-1 in conditioned medium (*CM*) from LYVE-1-transfected HT1080 cells. Full-length LYVE-1 was detected in the cell lysate (*Lys*). *D*, V5-tagged LYVE-1 expression vector (*upper panel*) was transfected into HT1080 cells. After TPA treatment (100 nM) for 30 min, the cell surface was labeled by biotinylation. The cell lysates were subjected to immunoprecipitation (*IP*) using anti-V5 antibody. Western blotting analysis was carried out with streptavidin-HRP. The cell lysates were analyzed by Western blotting with anti-LYVE-1 (C) antibody. Five micrograms of total cellular protein was loaded in each gel lane. *TM*, transmembrane; *AA*, amino acids.

overexpression of VEGF-A promotes cutaneous lymphangiogenesis as well as angiogenesis. Of interest, several lymphatic vessels lacked a continuous vessel wall in VEGF-A transgenic mice (Fig. 1*J*, *arrowheads*). Therefore, ear samples were further subjected to scanning electron microscopic analysis. Initial lymphatic vessels in wild-type mice demonstrated an oak leaf-like pattern of endothelial cell junctions as a typical feature of lymphatic capillaries (Fig. 1*K*). However, VEGF-A transgenic mice showed fenestration of the initial lymphatic vessels (Fig. 1*L*). Transmission electron microscopic analysis further confirmed the differential patterns of initial lymphatic endothelium. LECs revealed overlap in wild-type mice (Fig. 1*M*, *arrowheads*), whereas LECs in VEGF-A transgenic mice frequently lacked adequate overlap (Fig. 1*N*, *arrows*) and developed irregular attachments among the abnormal assembly by LECs (Fig. 1*N*, *arrowhead*). To clarify the exact localization of cell adhesion molecules in initial lymphatic vessels, we investigated the gap junction in initial lymphatic vessels. Double immunofluorescence analysis of the tight junction marker claudin-5 and LYVE-1 revealed that claudin-5 was prominently expressed at the beginning (Fig. 1*O*, *arrowhead*) and at the junction (Fig. 1*O*, *arrow*) of cutaneous initial lymphatic vessels in wild-type mice. In contrast, claudin-5 was broadly expressed in the initial lymphatic vessels of VEGF-A transgenic mice, and LYVE-1 expression was not clearly merged with claudin-5 in those vessels (Fig. 1*P*), indicating that a fragment of the LYVE-1 polypeptide might be localized in the extracellular space in response to VEGF-A overexpression.

Ectodomain Shedding of LYVE-1—To examine whether LYVE-1 shedding occurs or not, we used two antibodies against the N-terminal region and C-terminal region of LYVE-1 (Fig. 2*A*) and tested the effects of TPA, a potent inducer of membrane protein ectodomain shedding. Western blotting analysis indicated that TPA treatment of LYVE-1-transfected HT1080 cells resulted in the appearance of a CTF of LYVE-1 detected by anti-LYVE-1 (C) antibody (Fig. 2*B*, *right panel*, *white arrowhead*), and the band intensity of full-length LYVE-1 markedly decreased (Fig. 2*B*, *black arrowhead*). Next, conditioned media from HT1080 cells transfected with LYVE-1 were analyzed by Western blotting. After TPA treatment, the culture medium contained a soluble LYVE-1, which was shorter than full-length LYVE-1 (Fig. 2*C*, *white arrowhead*). To further confirm that LYVE-1 was cleaved from the surface of TPA-treated cells, we biotinylated cell surface proteins including LYVE-1 followed by immunoprecipitation and Western blotting. TPA treatment of HT1080 cells transfected with V5-tagged LYVE-1 (Fig. 2*D*, *upper schematic*) resulted in a down-regulation of cell surface LYVE-1 (Fig. 2*D*, *lower left panel*). A similar down-regulation was seen in the cell lysates detected by LYVE-1 (C) antibody (Fig. 2*D*, *lower right panel*). These results indicated that membrane-anchored LYVE-1 is cleaved by TPA treatment, and the LYVE-1 shedding generates soluble LYVE-1 peptides (Fig. 2*A*).

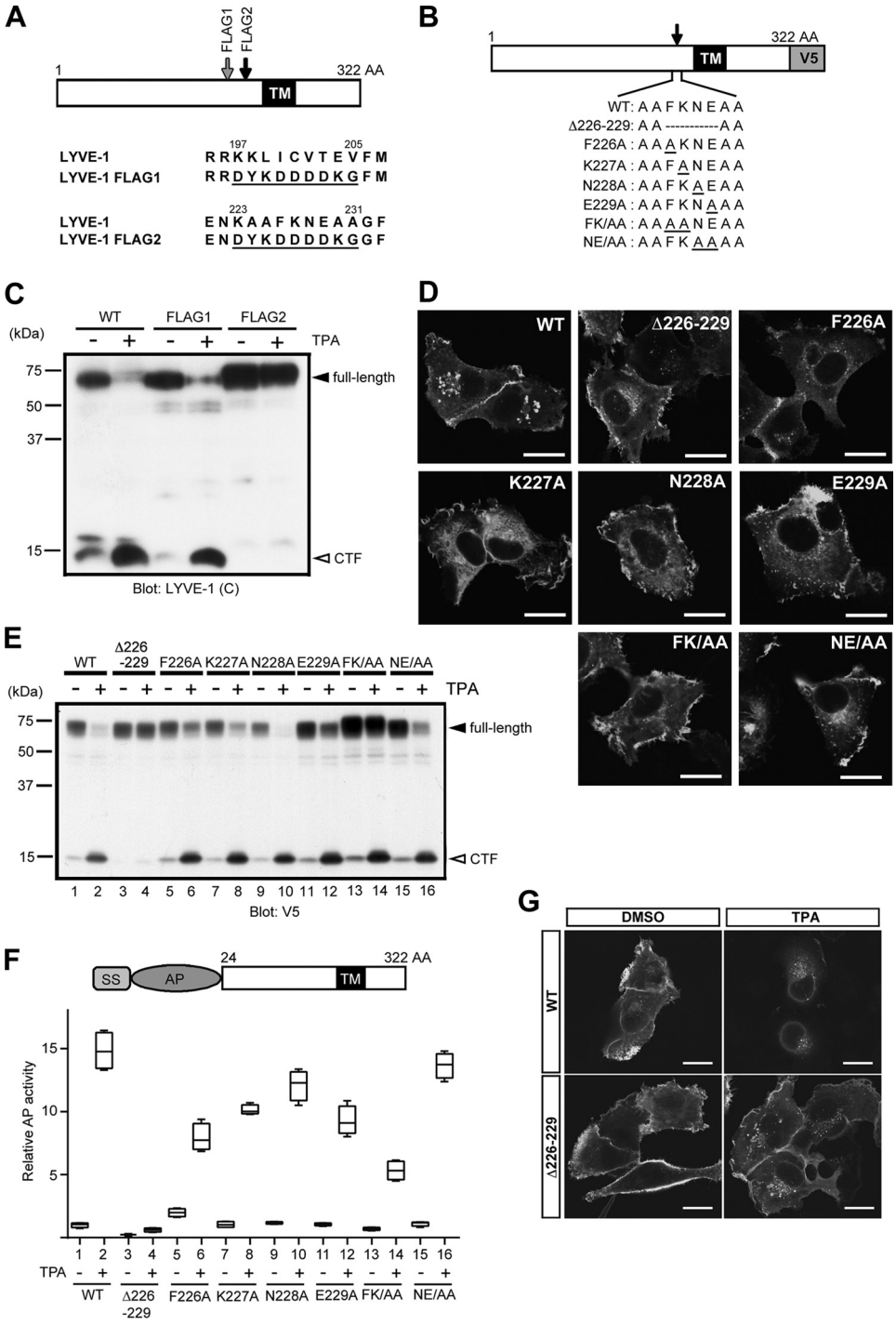

FIGURE 3. **Identification of the site responsible for LYVE-1 ectodomain shedding.** *A*, schematic representation of the two putative cleavage regions of LYVE-1. *TM*, transmembrane; *AA*, amino acids. Each LYVE-1 sequence (Lys^{197}–Val^{205} and Lys^{233}–Ala^{231}) was substituted by a FLAG sequence (*underlined*). *B*, schematic representation of deletion or amino acid substitution LYVE-1 mutants (*underlined*). *C*, Western blotting analysis of cell lysates derived from WT LYVE-1-, LYVE-1 FLAG1-, or LYVE-1 FLAG2-transfected HT1080 cells. After DMSO or TPA (100 nM) treatment for 30 min, the cell lysates were subjected to Western blotting analysis. Five micrograms of total cellular protein was loaded in each gel lane. *D*, HT1080 cells were transfected with WT or mutant LYVE-1 expression vectors. These cells were immunostained using an anti-V5 antibody. *Scale bar*, 20 μm. *E*, Western blotting analysis of cell lysates derived from WT or mutant LYVE-1-transfected HT1080 cells. After DMSO or TPA treatment, lysates were detected by anti-V5 antibody. Five micrograms of total cellular protein was loaded in each gel lane. *F*, schematic representation of AP-tagged LYVE-1 product (*upper*). *SS*, signal sequence. HT1080 cells were transfected with AP-LYVE-1 WT and AP-LYVE-1 mutants. After DMSO or TPA treatment, AP activity was analyzed in each medium. The experiment was performed independently in triplicate. Data are expressed as mean ± S.D. (*error bars*). *G*, HT1080 cells were transfected with WT or deletion mutant (Δ226–229). After DMSO or TPA treatment, these cells were immunostained using anti-LYVE-1 (N) antibody. *Scale bar*, 20 μm. *FK/AA*, F226A/K227A; *NE/AA*, N228A/E229A.

Identification of the Responsible Site for LYVE-1 Ectodomain Shedding—To gain information about the cleavage site of LYVE-1 ectodomain shedding, we made several LYVE-1 mutants (Fig. 3, *A* and *B*). Because the two cleavage sites of CD44 have been reported (20), we compared the amino acid sequence of LYVE-1 with that of CD44 and found two puta-

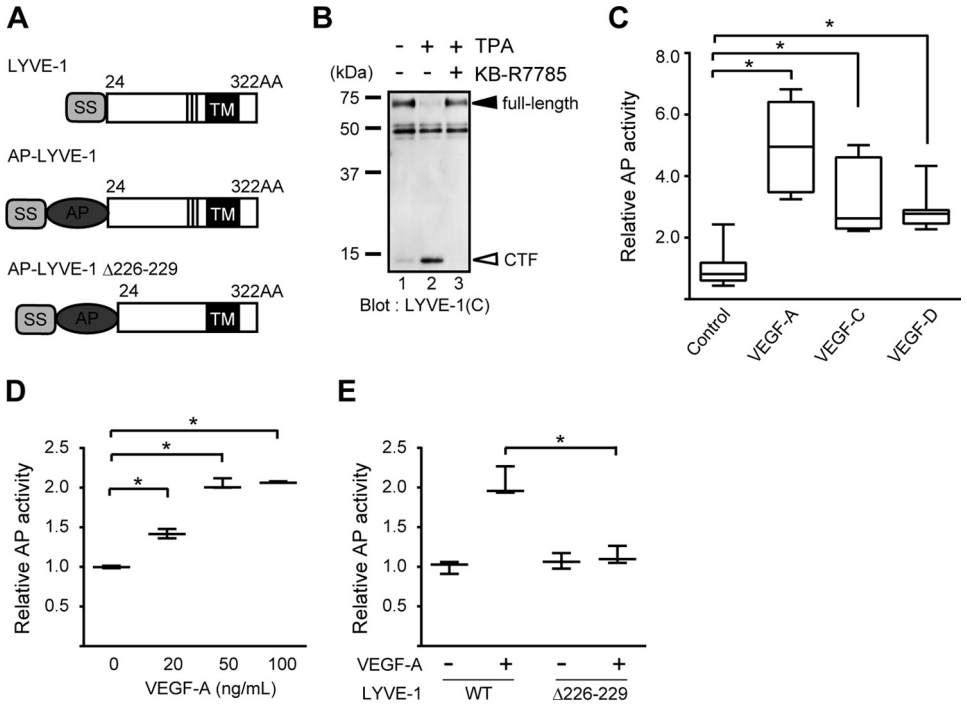

FIGURE 4. **VEGF-A potently promotes LYVE-1 ectodomain shedding in LECs.** *A*, schematic representation of AP-tagged LYVE-1 or the deletion form of LYVE-1 (Δ226–229). *SS*, signal sequence; *TM*, transmembrane; *AA*, amino acids. *B*, Western blotting analysis of the cell lysates from LECs. LECs were infected with adenoviruses encoding LYVE-1. After 24 h, LECs were incubated with DMSO or TPA (100 nM) for 30 min. KB-R7785 (20 μM) was incubated for 30 min before TPA treatment. Ten micrograms of total cellular protein was loaded in each gel lane. *C*, LECs were infected with adenoviruses encoding AP-LYVE-1. After 6 h of serum starvation, LECs were incubated with VEGF-A (50 ng/ml), VEGF-C (500 ng/ml), or VEGF-D (500 ng/ml) for 6 h. The AP activities were analyzed in each medium. *D*, VEGF-A induced LYVE-1 shedding in a dose-dependent manner. The AP assay was performed as in *C*. *E*, LECs were infected with adenoviruses encoding AP-LYVE-1 or AP-LYVE-1 Δ226–229. The AP assay was performed as in *C*. All experiments were performed independently in triplicate. *, $p < 0.05$. Data are expressed as mean ± S.D. (*error bars*).

tive cleavage sites of LYVE-1 (Ile^{200}-Cys^{201} and Phe^{226}-Lys^{227}). To confirm the involvement of these sites in LYVE-1 shedding, each putative cleavage site was substituted by a FLAG sequence (Fig. 3*A*). Western blotting analysis indicated that the replacement of amino acids from residue 223–231 with a FLAG sequence (LYVE-1 FLAG2) completely blocked LYVE-1 shedding, whereas another mutant, residues 197–205 with FLAG (LYVE-1 FLAG1), did not (Fig. 3*C*). To further analyze the LYVE-1 cleavage site in detail, we made several mutants that have deletion or amino acid substitution around the putative cleavage site (Fig. 3*B*). The mutated and wild-type (WT) forms of LYVE-1 were located at the plasma membrane (Fig. 3*D*). Western blotting analysis indicated that the shedding of the four amino acid substitution mutants (F226A, K227A, E229A, F226A/K227A, and N228A/E229A) led to decreased shedding efficiency when compared with WT (Fig. 3*E*, *lanes 5–16*). To quantitate the degree of resistance of these LYVE-1 mutants against TPA-induced shedding, we constructed several expression vectors encoding human placental AP-tagged LYVE-1 (WT and mutants) (Fig. 3*F*). This approach has been used previously to evaluate the ectodomain shedding of EGF receptor ligands (16, 21). When HT1080 cells were transfected with AP-tagged LYVE-1 (WT), shedding of LYVE-1 was strongly induced after addition of TPA (Fig. 3*F*, *lane 2*), consistent with the Western blotting analysis (Fig. 3, *C* and *E*). Both basal shedding and TPA-induced shedding were mostly inhibited by the amino acid deletion (Δ226–229) (Fig. 3*F*, *lanes 3* and *4*). The degree of TPA-induced shedding of amino acid substitution mutants (F226A, K227A, N228A, E229A, and F226A/K227A) also decreased when compared with WT (Fig. 3*F*, *lanes 6*, *8*, *10*, *12*, and *14*). Immunostaining using anti-LYVE-1 (N) antibody showed that after TPA treatment, WT LYVE-1 disappeared from the cell surface, whereas deletion mutants (Δ226–229) continued to locate on the plasma membrane (Fig. 3*G*). Taken together, our results suggest that the region of Phe^{226}–Glu^{229} is responsible for LYVE-1 ectodomain shedding, and the deletion mutant (Δ226–229) is cleavage-resistant and therefore termed the uncleavable LYVE-1.

VEGF Induces LYVE-1 Ectodomain Shedding in Lymphatic Endothelial Cells—Next, to examine the LYVE-1 shedding in cultured human LECs, we initially constructed an adenoviral vector encoding LYVE-1 or AP-tagged LYVE-1 fusion protein with or without the responsible element (Phe^{226}–Glu^{229}) for ectodomain shedding (Fig. 4*A*). We transfected the LYVE-1 adenovirus to LECs that were incubated with or without TPA. Western blotting analysis revealed that TPA treatment induced LYVE-1 shedding in LECs (Fig. 4*B*, *lanes 1* and *2*). This analysis also showed that LYVE-1 shedding was inhibited by the metalloprotease inhibitor KB-R7785 in LECs (Fig. 4*B*, *lane 3*), indicating that LYVE-1 shedding is mediated by metalloproteases.

Because VEGF-C and VEGF-D are known as major lymphangiogenesis factors and VEGF-A also promotes lymphangiogenesis, we next examined their effects in the AP assay. LYVE-1 shedding was enhanced by recombinant VEGF-C and VEGF-D at 500 ng/ml, whereas the levels of shedding were strongly enhanced by recombinant VEGF-A at 50

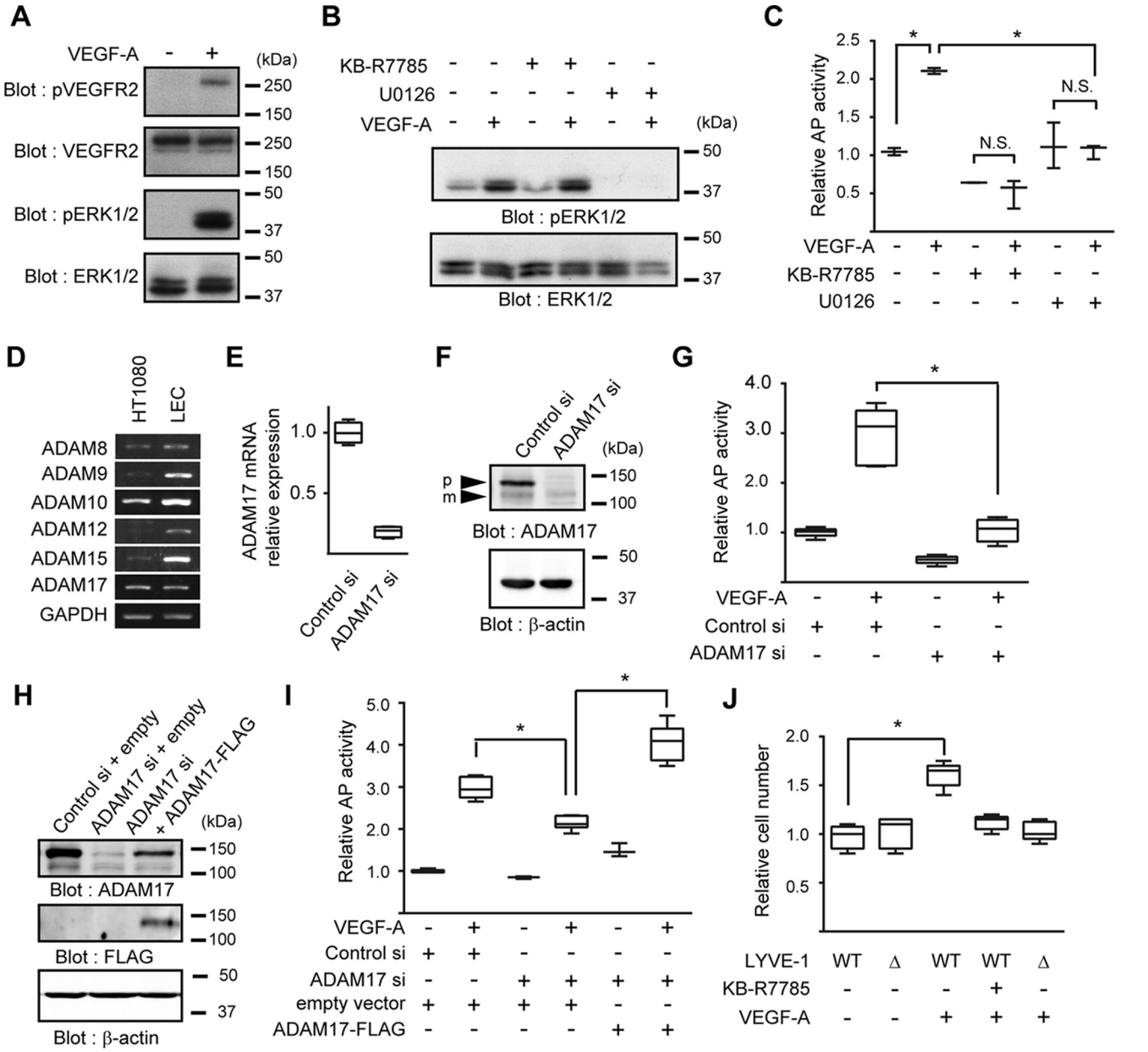

FIGURE 5. **Mitogen-activated protein kinase pathway and ADAM17 are responsible for VEGF-A-induced LYVE-1 shedding.** *A*, Western blotting analysis showed phosphorylation of VEGFR-2 and ERK1/2 in LECs after 5 min of VEGF-A stimulation. Ten micrograms of total cellular protein was loaded in each gel lane. *B*, validation of chemical inhibitors in LECs by Western blotting analysis. LECs were treated with KB-R7785 (20 μM) or U0126 (10 μM) for 30 min. After 5 min of VEGF-A stimulation, the cell lysates were subjected to Western blotting analysis. Ten micrograms of total cellular protein was loaded in each gel lane. *C*, after 6 h of VEGF-A stimulation, AP activity was analyzed in conditioned media from LECs cultured in the presence or absence of U0126 (10 μM) or KB-R7785 (20 μM). *D*, semiquantitative RT-PCR analysis revealed that ADAM17 is expressed in LECs and HT1080 cells. *E*, quantitative RT-PCR analyses of knockdown of ADAM17 by siRNA transfection in LECs. *F*, Western blotting analysis of ADAM17 knockdown in LECs. Ten micrograms of total cellular protein was loaded in each gel lane. *p*, pro-form ADAM17; *m*, mature form ADAM17. *G*, after 6 h VEGF-A stimulation, AP activity was analyzed in conditioned media from LECs transfected with individual siRNAs. *H*, Western blotting analysis of knockdown and re-expression of ADAM17 in HUVECs. Ten micrograms of total cellular protein was loaded in each gel lane. *I*, after 6 h of VEGF-A stimulation, AP activity was analyzed in conditioned media from HUVECs transfected with individual siRNAs and vectors. *J*, haptotactic LEC migration assay showed that LYVE-1 ectodomain shedding contributed to haptotaxis of LECs toward VEGF-A. All experiments were performed independently in triplicate. *, $p < 0.05$; *N.S.*, not significant. Data are expressed as mean ± S.D. (*error bars*).

ng/ml (Fig. 4*C*). This result indicated that VEGF-A potently promotes the ectodomain shedding of LYVE-1 in LECs. Because VEGF-A-induced LYVE-1 shedding was dose-dependent up to 50 ng/ml (Fig. 4*D*), we utilized VEGF-A at 50 ng/ml in subsequent experiments. The deletion of amino acid sequence Phe^{226}–Glu^{229} from AP-tagged LYVE-1 led to no enhancement of shedding even in the presence of VEGF-A (Fig. 4*E*), indicating that the amino acid sequence Phe^{226}–Glu^{229} is also responsible for the VEGF-A-induced LYVE-1 ectodomain shedding in LECs.

LYVE-1 Shedding Depends on ERK Signaling and ADAM17—To explore downstream mechanisms involved in VEGF-A-induced LYVE-1 shedding, we used chemical compounds that inhibit the LYVE-1 shedding. In LECs, VEGF-A induced phosphorylation of VEGFR-2 and ERK1/2, one of the major downstream components of the VEGFR-2 pathway (Fig. 5, *A* and *B*).

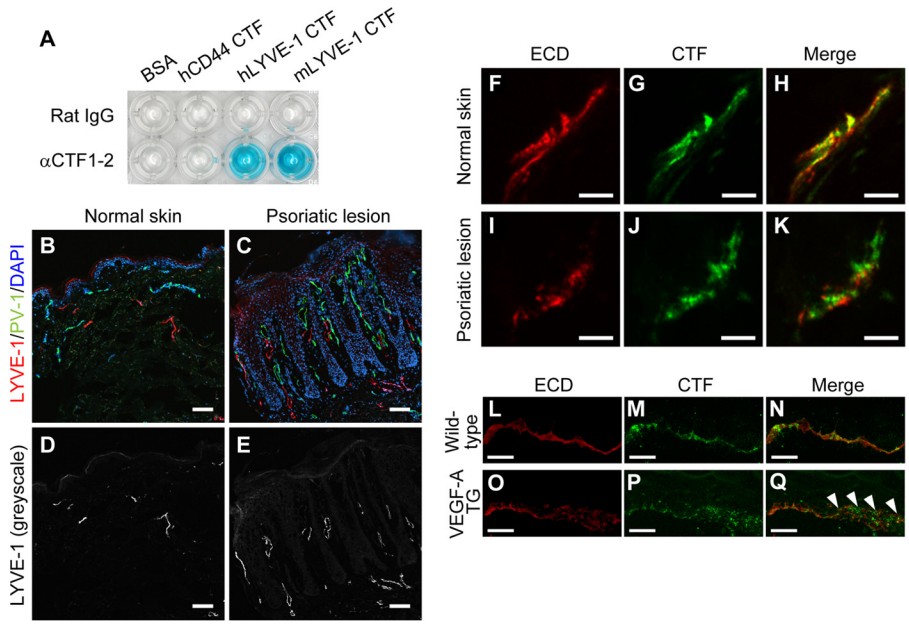

FIGURE 6. **Expression patterns of LYVE-1 in psoriasis skin.** *A*, ELISA analysis revealed reactivity against human (*hLYVE-1*) and mouse LYVE-1 (*mLYVE-1*) CTF but not against human CD44 (*hCD44*) CTF. *B* and *C*, double immunofluorescence analysis for LYVE-1 (*red*) and PV-1 (*green*) in normal (*A*) and psoriatic human skin (*B*). Nuclei were stained by DAPI (*blue*). *Scale bar*, 100 μm. *D* and *E*, immunofluorescence staining for LYVE-1 (*grayscale*) in normal (*D*) and psoriatic human skin (*E*). *Scale bar*, 100 μm. *F–K*, double immunofluorescence staining for the extracellular domain (*ECD*; *red*) and CTF (*green*) of LYVE-1 in normal and psoriasis skin. *Scale bar*, 30 μm. *L–Q*, double immunofluorescence staining for the extracellular domain (*red*) and CTF (*green*) of LYVE-1 in wild-type and VEGF-A transgenic (*TG*) mouse skin. *Scale bar*, 10 μm.

Pretreatment with U0126, an ERK kinase inhibitor, repressed the phosphorylation of ERK1/2 (Fig. 5*B*) and blocked VEGF-A-stimulated LYVE-1 shedding (Fig. 5*C*). Furthermore, pretreatment with the metalloprotease inhibitor KB-R7785 did not affect the phosphorylation of ERK1/2 (Fig. 5*B*) but significantly decreased VEGF-A-induced LYVE-1 shedding in LECs (Fig. 5*C*). These results indicated that VEGF-A-induced LYVE-1 shedding is mediated through a VEGFR-2/ERK signal pathway that activates the metalloproteases.

Among the metalloproteases, a family of ADAM is known to induce the ectodomain shedding of several transmembrane proteins such as CD44. Semiquantitative reverse transcription (RT)-PCR analysis showed that the mRNA level of ADAM17 is prominent both in HT1080 and LECs (Fig. 5*D*). To examine whether ADAM17 is responsible for LYVE-1 ectodomain shedding, we used siRNA to knock down ADAM17 in LECs. Real time quantitative RT-PCR and Western blotting analysis showed that ADAM17 expression was effectively suppressed by siRNA transfection (Fig. 5, *E* and *F*). The AP-tagged shedding assay revealed that VEGF-A-induced LYVE-1 shedding was significantly decreased in LECs when the cells underwent ADAM17 knockdown (Fig. 5*G*). To exclude the possibility that the effect was induced by off-target effects of the transfected siRNA, we performed an siRNA rescue experiment. The culture system of LECs, however, has a significant limitation, namely a low transfection efficiency of expression plasmids. To circumvent this problem, we utilized HUVECs and overexpressed siRNA-resistant ADAM17 in these cells. Knockdown of ADAM17 in HUVECs also suppressed VEGF-A-induced LYVE-1 shedding, which was rescued by the re-expression of siRNA-resistant ADAM17-FLAG (Fig. 5, *H* and *I*). Taken together, these results confirm ADAM17 as the sheddase of LYVE-1.

LYVE-1 Ectodomain Shedding Is Required for VEGF-A-induced Migration of LEC—To clarify the biological relevance of LYVE-1 shedding, we investigated haptotactic LEC migration toward VEGF-A. Transwell migration assays using hyaluronic acid-coated membranes showed that the number of migrated LECs was comparable with WT and with uncleavable LYVE-1 in the absence of VEGF-A (Fig. 5*J*). Notably, WT LYVE-1 promoted cell migration in response to VEGF-A, whereas pretreatment with KB-R7785 markedly inhibited the cell migration (Fig. 5*J*). Uncleavable LYVE-1 was unable to induce cell migration (Fig. 5*J*). These results indicate that the proteolytic cleavage of LYVE-1 is required for enhanced LEC migration toward VEGF-A.

Expression Patterns of LYVE-1 in Lymphatic Endothelial Cells of Psoriasis—Finally, to address the question whether LYVE-1 shedding occurs during pathological lymphangiogenesis in human skin diseases, we histologically investigated psoriasis lesions using antibodies against either the extracellular or cytoplasmic domain of LYVE-1. Because no specific antibody was available to histologically label the cytoplasmic region of LYVE-1, we generated a hybridoma cell line CTF1-2 that produces a monoclonal antibody against the LYVE-1 CTF. An enzyme-linked immunosorbent assay revealed that the novel antibody reacts with both human and mouse peptides of LYVE-1 CTF, whereas no cross-reactivity was found against human CD44 CTF (Fig. 6*A*).

Psoriasis is known to induce pathological lymphangiogenesis as well as angiogenesis, which was confirmed by double immunofluorescence analyses for LYVE-1 and for PV-1 as compared with normal human skin (Fig. 6, *B–E*). In normal skin, CTF1-2 accurately recognized human dermal lymphatic vessels, which were stained with the commercially available anti-LYVE-1 antibody against the N-terminal region (Fig. 6, *F–H*). This evalua-

tion revealed that CTF1-2 specifically reacts with LYVE-1 in the immunofluorescence analysis. Furthermore, the double immunofluorescence analysis revealed that the respective LYVE-1 stainings were completely merged in lymphatic vessels in normal skin (Fig. 6, *F–H*) but not in psoriatic lesions (Fig. 6, *I–K*). Likewise, double immunofluorescence analyses revealed that the respective LYVE-1 stainings were merged in normal mice (Fig. 6, *L–N*), whereas distinct expression patterns of LYVE-1 were observed in VEGF-A transgenic mouse skin (Fig. 6, *O–Q*, *arrowheads*). These immunofluorescence analyses suggested that the LYVE-1 CTF peptide was displaced from the extracellular region of LYVE-1 or that the epitope of CTF1-2 was masked by cytoplasmic interacting molecules specifically in psoriasis and VEGF-A transgenic mouse skin. Our biochemical analyses at least support the former possibility, that is that LYVE-1 might undergo ectodomain shedding in psoriasis lesions.

Discussion

This is the first report describing the proteolytic cleavage of LYVE-1 induced by VEGF-A in LECs. LYVE-1 is a receptor for hyaluronic acid, one of the most prominent extracellular matrix molecules in the skin. CD44, the other cell surface receptor for hyaluronic acid, is capable of promoting the migration of tumor cells by ectodomain shedding (14). Furthermore, CD44 cleavage was found in several human tumors including glioblastomas, whereas no proteolytic products were found in normal tissue (22), indicating that CD44 ectodomain shedding occurs in certain pathological conditions such as tumor progression. Therefore, it is conceivable that LYVE-1 is also biochemically cleaved during pathological lymphangiogenesis so that LECs can decrease cell matrix adhesion and increase their potency for migration. In the present study, an overlapping immunohistological staining for the extracellular and intracellular domains of LYVE-1 was found in normal lymphatic vessels, whereas this overlap was not observed in lymphatic vessels associated with psoriasis. Thus, the ectodomain shedding of LYVE-1 might contribute to the pathogenesis of psoriasis by promoting haptotactic migration of LECs toward VEGF-A.

Our present study reveals that VEGF-A induces the activation of ADAM17, leading to the proteolytic cleavage of LYVE-1 in LECs. ADAM17 is an important factor for processing of several angiogenesis-related factors such as VEGFR-2, vascular endothelial cadherin, and platelet endothelial cell adhesion molecule in endothelial cells (16). A recent study reported that ADAM17 in endothelial cells has a role in pathological neovascularization, whereas conditional knock-out of ADAM17 in endothelium had no effect on development and adult homeostasis (16, 23). This result is consistent with our immunohistological analysis of normal and psoriasis tissues and supports our proposal that ectodomain shedding of LYVE-1 is induced during chronic inflammation such as psoriasis.

We provide evidence for a novel molecular mechanism for generating a soluble form of LYVE-1. A recent study indicated that soluble LYVE-1 may interfere with migration and proliferation of LECs by binding directly to fibroblast growth factor-2 (FGF-2) *in vitro* and *in vivo* (24). FGF-2 and VEGF-C collaboratively promote tumor growth, angiogenesis, intratumoral lymphangiogenesis, and metastasis (25). Furthermore, serum levels of FGF-2 in psoriasis patients were relatively high compared with those in healthy blood donors (26). LYVE-1 ectodomain shedding was also induced by FGF-2 as well as VEGF-A in cultured LECs (data not shown). Future studies will be needed to examine whether ectodomain shedding of LYVE-1 plays a key role in promoting lymphangiogenesis under pathological conditions such as psoriasis.

Author Contributions—H. N.-F. and S. Hirakawa designed and performed most experiments and wrote the manuscript. R. A. and Y. T. generated the monoclonal antibody against LYVE-1. M. S. performed electron microscopic analyses. S. Higashiyama, H. O., H. N., S. F., T. S., Y. S., K. S., K. H., and M. D. helped with data acquisition and provided critical materials. All authors analyzed the results and approved the final version of the manuscript.

Acknowledgments—We thank T. Tsuda, E. Tan, K. Ando, C. Tada-Seno, H. Iwabuki, and N. Matsushita for excellent technical assistance and Dr. Dontscho Kerjaschki for helpful discussions.

References

1. Wigle, J. T., and Oliver, G. (1999) Prox1 function is required for the development of the murine lymphatic system. *Cell* **98,** 769–778
2. Karkkainen, M. J., Haiko, P., Sainio, K., Partanen, J., Taipale, J., Petrova, T. V., Jeltsch, M., Jackson, D. G., Talikka, M., Rauvala, H., Betsholtz, C., and Alitalo, K. (2004) Vascular endothelial growth factor C is required for sprouting of the first lymphatic vessels from embryonic veins. *Nat. Immunol.* **5,** 74–80
3. Detmar, M., Brown, L. F., Claffey, K. P., Yeo, K. T., Kocher, O., Jackman, R. W., Berse, B., and Dvorak, H. F. (1994) Overexpression of vascular permeability factor/vascular endothelial growth factor and its receptors in psoriasis. *J. Exp. Med.* **180,** 1141–1146
4. Detmar, M., Brown, L. F., Schön, M. P., Elicker, B. M., Velasco, P., Richard, L., Fukumura, D., Monsky, W., Claffey, K. P., and Jain, R. K. (1998) Increased microvascular density and enhanced leukocyte rolling and adhesion in the skin of VEGF transgenic mice. *J. Invest. Dermatol.* **111,** 1–6
5. Kajiya, K., Hirakawa, S., and Detmar, M. (2006) Vascular endothelial growth factor-A mediates ultraviolet B-induced impairment of lymphatic vessel function. *Am. J. Pathol.* **169,** 1496–1503
6. Hirakawa, S., Kodama, S., Kunstfeld, R., Kajiya, K., Brown, L. F., and Detmar, M. (2005) VEGF-A induces tumor and sentinel lymph node lymphangiogenesis and promotes lymphatic metastasis. *J. Exp. Med.* **201,** 1089–1099
7. Nagy, J. A., Vasile, E., Feng, D., Sundberg, C., Brown, L. F., Detmar, M. J., Lawitts, J. A., Benjamin, L., Tan, X., Manseau, E. J., Dvorak, A. M., and Dvorak, H. F. (2002) Vascular permeability factor/vascular endothelial growth factor induces lymphangiogenesis as well as angiogenesis. *J. Exp. Med.* **196,** 1497–1506
8. Huggenberger, R., Ullmann, S., Proulx, S. T., Pytowski, B., Alitalo, K., and Detmar, M. (2010) Stimulation of lymphangiogenesis via VEGFR-3 inhibits chronic skin inflammation. *J. Exp. Med.* **207,** 2255–2269
9. Banerji, S., Ni, J., Wang, S. X., Clasper, S., Su, J., Tammi, R., Jones, M., and Jackson, D. G. (1999) LYVE-1, a new homologue of the CD44 glycoprotein, is a lymph-specific receptor for hyaluronan. *J. Cell Biol.* **144,** 789–801
10. Hirakawa, S., Hong, Y. K., Harvey, N., Schacht, V., Matsuda, K., Libermann, T., and Detmar, M. (2003) Identification of vascular lineage-specific genes by transcriptional profiling of isolated blood vascular and lymphatic endothelial cells. *Am. J. Pathol.* **162,** 575–586
11. Hirakawa, S. (2011) Regulation of pathological lymphangiogenesis requires factors distinct from those governing physiological lymphangiogenesis. *J. Dermatol. Sci.* **61,** 85–93
12. Huang, S. S., Liu, I. H., Smith, T., Shah, M. R., Johnson, F. E., and Huang,

J. S. (2006) CRSBP-1/LYVE-l-null mice exhibit identifiable morphological and functional alterations of lymphatic capillary vessels. *FEBS Lett.* **580,** 6259–6268
13. Gale, N. W., Prevo, R., Espinosa, J., Ferguson, D. J., Dominguez, M. G., Yancopoulos, G. D., Thurston, G., and Jackson, D. G. (2007) Normal lymphatic development and function in mice deficient for the lymphatic hyaluronan receptor LYVE-1. *Mol. Cell. Biol.* **27,** 595–604
14. Nagano, O., and Saya, H. (2004) Mechanism and biological significance of CD44 cleavage. *Cancer Sci.* **95,** 930–935
15. Higashiyama, S., Iwabuki, H., Morimoto, C., Hieda, M., Inoue, H., and Matsushita, N. (2008) Membrane-anchored growth factors, the epidermal growth factor family: beyond receptor ligands. *Cancer Sci.* **99,** 214–220
16. Weskamp, G., Mendelson, K., Swendeman, S., Le Gall, S., Ma, Y., Lyman, S., Hinoki, A., Eguchi, S., Guaiquil, V., Horiuchi, K., and Blobel, C. P. (2010) Pathological neovascularization is reduced by inactivation of ADAM17 in endothelial cells but not in pericytes. *Circ. Res.* **106,** 932–940
17. Nagano, O., Murakami, D., Hartmann, D., De Strooper, B., Saftig, P., Iwatsubo, T., Nakajima, M., Shinohara, M., and Saya, H. (2004) Cell-matrix interaction via CD44 is independently regulated by different metalloproteinases activated in response to extracellular Ca^{2+} influx and PKC activation. *J. Cell Biol.* **165,** 893–902
18. Hirakawa, S., Brown, L. F., Kodama, S., Paavonen, K., Alitalo, K., and Detmar, M. (2007) VEGF-C-induced lymphangiogenesis in sentinel lymph nodes promotes tumor metastasis to distant sites. *Blood* **109,** 1010–1017
19. Tomono, Y., Naito, I., Ando, K., Yonezawa, T., Sado, Y., Hirakawa, S., Arata, J., Okigaki, T., and Ninomiya, Y. (2002) Epitope-defined monoclonal antibodies against multiplexin collagens demonstrate that type XV and XVIII collagens are expressed in specialized basement membranes. *Cell Struct. Funct.* **27,** 9–20
20. Nakamura, H., Suenaga, N., Taniwaki, K., Matsuki, H., Yonezawa, K., Fujii, M., Okada, Y., and Seiki, M. (2004) Constitutive and induced CD44 shedding by ADAM-like proteases and membrane-type 1 matrix metalloproteinase. *Cancer Res.* **64,** 876–882
21. Nakayama, H., Fukuda, S., Inoue, H., Nishida-Fukuda, H., Shirakata, Y., Hashimoto, K., and Higashiyama, S. (2012) Cell surface annexins regulate ADAM-mediated ectodomain shedding of proamphiregulin. *Mol. Biol. Cell* **23,** 1964–1975
22. Okamoto, I., Tsuiki, H., Kenyon, L. C., Godwin, A. K., Emlet, D. R., Holgado-Madruga, M., Lanham, I. S., Joynes, C. J., Vo, K. T., Guha, A., Matsumoto, M., Ushio, Y., Saya, H., and Wong, A. J. (2002) Proteolytic cleavage of the CD44 adhesion molecule in multiple human tumors. *Am. J. Pathol.* **160,** 441–447
23. Lucitti, J. L., Mackey, J. K., Morrison, J. C., Haigh, J. J., Adams, R. H., and Faber, J. E. (2012) Formation of the collateral circulation is regulated by vascular endothelial growth factor-A and a disintegrin and metalloprotease family members 10 and 17. *Circ. Res.* **111,** 1539–1550
24. Platonova, N., Miquel, G., Regenfuss, B., Taouji, S., Cursiefen, C., Chevet, E., and Bikfalvi, A. (2013) Evidence for the interaction of fibroblast growth factor-2 with the lymphatic endothelial cell marker LYVE-1. *Blood* **121,** 1229–1237
25. Cao, R., Ji, H., Feng, N., Zhang, Y., Yang, X., Andersson, P., Sun, Y., Tritsaris, K., Hansen, A. J., Dissing, S., and Cao, Y. (2012) Collaborative interplay between FGF-2 and VEGF-C promotes lymphangiogenesis and metastasis. *Proc. Natl. Acad. Sci. U.S.A.* **109,** 15894–15899
26. Andrys, C., Borska, L., Pohl, D., Fiala, Z., Hamakova, K., and Krejsek, J. (2007) Angiogenic activity in patients with psoriasis is significantly decreased by Goeckerman's therapy. *Arch. Dermatol. Res.* **298,** 479–483